ARTICLE

The novel pre-rRNA detection workflow "Riboprobing" allows simple identification of undescribed RNA species

MAGDALENA GERHALTER,[1] LISA KOFLER,[1] GERTRUDE ZISSER,[1] JULIANE MERL-PHAM,[2] STEFANIE M. HAUCK,[2] and HELMUT BERGLER[1,3]

[1]Institute of Molecular Biosciences, University of Graz, Graz 8010, Austria
[2]Metabolomics and Proteomics Core, Helmholtz Center Munich, Munich 80939, Germany
[3]BioTechMed-Graz, Graz 8010, Austria

ABSTRACT

Ribosomes translate mRNA into proteins and are essential for every living organism. In eukaryotes, both ribosomal subunits are rapidly assembled in a strict hierarchical order, starting in the nucleolus with the transcription of a common precursor ribosomal RNA (pre-rRNA). This pre-rRNA encodes three of the four mature rRNAs, which are formed by several, consecutive endonucleolytic and exonucleolytic processing steps. Historically, northern blots are used to analyze the variety of different pre-rRNA species, only allowing rough length estimations. Although this limitation can be overcome with primer extension, both approaches often use radioactivity and are time-consuming and costly. Here, we present "Riboprobing," a linker ligation-based workflow followed by reverse transcription and PCR for easy and fast detection and characterization of pre-rRNA species and their 5′ as well as 3′ ends. Using standard molecular biology laboratory equipment, "Riboprobing" allows reliable discrimination of pre-rRNA species not resolved by northern blot (e.g., 27SA$_2$, 27SA$_3$, and 27SB pre-rRNA). The method can successfully be used for the analysis of total cell extracts as well as purified pre-ribosomes for a straightforward evaluation of the impact of mutant gene versions or inhibitors. In the course of method development, we identified and characterized a hitherto undescribed aberrant pre-rRNA arising from LiCl inhibition. This pre-rRNA fragment spans from processing site A1 to E, forming a small RNP that lacks most early joining assembly factors. This finding expands our knowledge of how the cell deals with severe pre-rRNA processing defects and demonstrates the strict requirement for the 5′ETS (external transcribed spacer) for the assembly process.

Keywords: ribosome biogenesis; pre-rRNA processing; primer extension; reverse transcription; aberrant pre-rRNA

INTRODUCTION

Every dividing cell depends on a pool of correctly assembled ribosomes. Eukaryotic ribosomes consist of four ribosomal RNAs (rRNAs) and around 80 ribosomal proteins (r-proteins). Their assembly follows a strictly coordinated maturation cascade which is best understood in the yeast *Saccharomyces cerevisiae* where it involves approximately 250 maturation factors (for review, see Baßler and Hurt 2019; Klinge and Woolford 2019; Dörner et al. 2023). Because of the high conservation of the ribosomal architecture, the assembly of human ribosomes follows the same principles as described in yeast (Ni et al. 2022; Dörner et al. 2023; Durand et al. 2023).

In the nucleolus, ribosome biogenesis starts by RNA polymerase I (Pol I) transcribing the 35S precursor ribosomal RNA (pre-rRNA) that comprises the mature 18S, 5.8S, and 25S rRNAs (in the case of *S. cerevisiae*), flanked by external transcribed spacers (5′ETS and 3′ETS) and separated by internal transcribed spacers (ITS1 between 18S and 5.8S rRNA and ITS2 between 5.8S and 25S rRNA) (Fig. 1A, uppermost part). During ribosome maturation these ETS and ITS regions are removed by several endo- and exonucleolytic processing steps that are coordinated with excessive rRNA folding and modifications events (Fig. 1A; for review, see Sloan et al. 2017; Tomecki et al. 2017; Mitterer and Pertschy 2022; Schneider and Bohnsack 2023).

UTP-A, UTP-B, the U3 snoRNP and UTP-C join the emerging 35S pre-rRNA cotranscriptionally. First, a 5′ETS particle is assembled, followed by the formation of the 90S pre-ribosome (Supplemental Fig. S1A; Osheim et al. 2004; Hunziker et al. 2019). In the 90S pre-ribosome,

Corresponding author: helmut.bergler@uni-graz.at
Handling editor: John Woolford
Article is online at http://www.rnajournal.org/cgi/doi/10.1261/rna.079912.123. Freely available online through the *RNA* Open Access option.

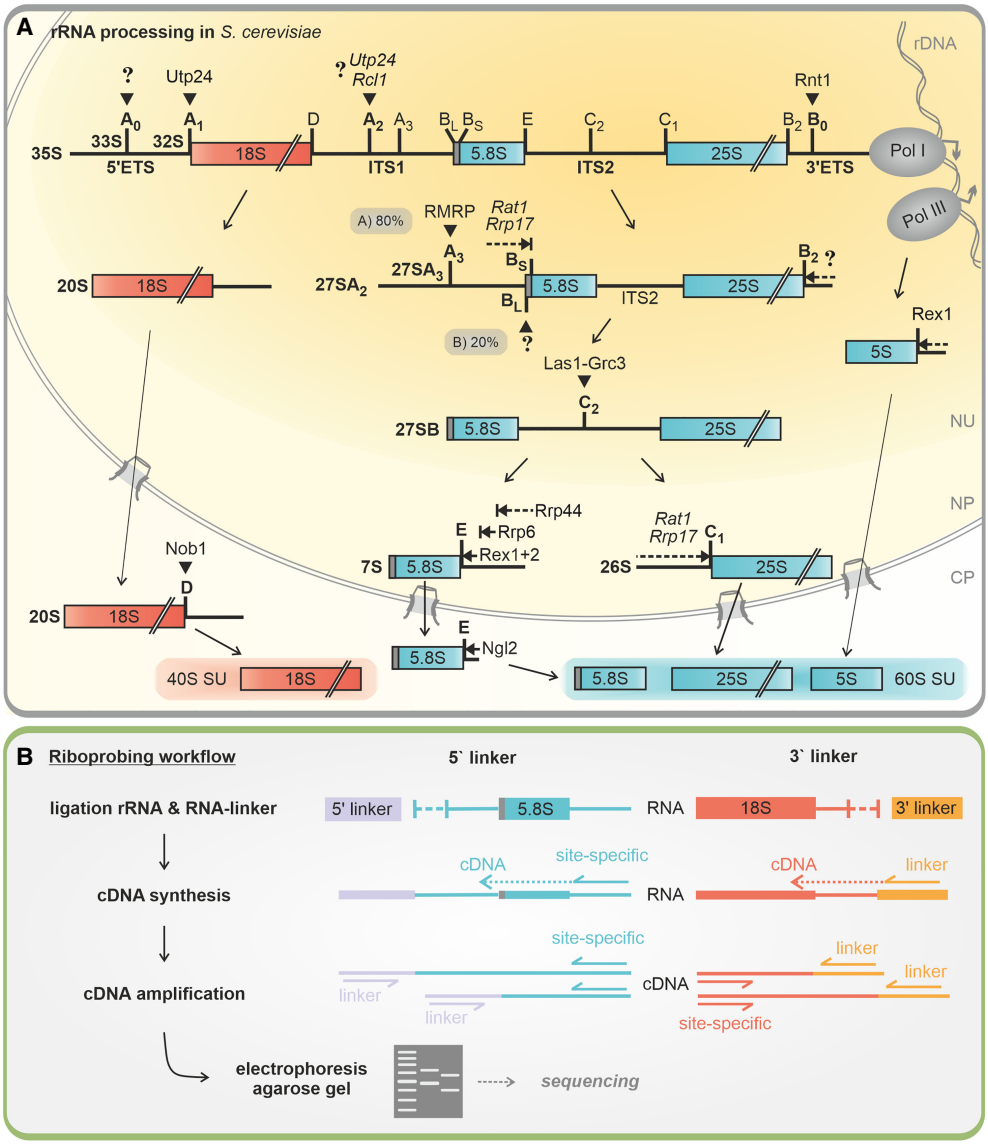

FIGURE 1. (*A*) Processing of the precursor ribosomal RNA (rRNA) to the four mature rRNAs. Blue boxes indicate large subunit rRNAs (60S SU) and red boxes mark the small subunit rRNA (40S SU). The 35S precursor rRNA still harbors the two flanking regions 5′ETS and 3′ETS (external transcribed spacers) and the two internal transcribed spacer elements ITS1 and 2. Endonucleolytic cleavage sites (▼) and regions removed by exonucleolytic trimming (→) are labeled. Enzymes in italics indicate candidate proteins involved in processing or when several enzymes were described to act at the same site. For processing sites with question marks, no enzyme was identified until now. (NU) Nucleolus, (NP) nucleoplasm, (CP), cytoplasm. (*B*) Experimental design of the Riboprobing workflow. At first, an RNA linker is ligated to isolated RNA. Depending on whether the 3′ or the 5′ end is investigated, a different primer serves as the starting point of the reverse transcription. For the 5′ end, a site-specific primer is chosen (e.g., the C_1C_2 primer that allows discrimination of the different 27S pre-rRNA species). For the 3′ ends, the primer hybridizing to the linker (linker primer) is used to initiate cDNA synthesis. In the next step, the cDNA is amplified. For the 5′ ends, the primer used for cDNA synthesis is combined with a primer hybridizing to the linker. To investigate the 3′ ends, the linker primer is combined with a primer defining the region of interest, in this scheme the 3′ end of the 18S rRNA. Amplified DNA fragments are separated in agarose gels to deduce which pre-rRNA species were present in the sample.

cleavage at site A0 is followed by cleavage at site A1 by Utp24, which forms the mature 5′ end of the 18S rRNA (Dragon et al. 2002; Bleichert et al. 2006; Wells et al. 2016; Khoshnevis et al. 2019). The mature 3′ end of the 18S rRNA is only formed in the cytoplasm by cleavage at site D by the endonuclease Nob1 (Fig. 1A; Fatica et al. 2003, 2004; Pertschy et al. 2009; Heuer et al. 2017).

Most pre-rRNA transcripts are cleaved cotranscriptionally at site A2 (Koš and Tollervey 2010) either by Utp24 (Bleichert et al. 2006) or by Rcl1 (Horn et al. 2011; Delprato et al. 2014). This separates the maturation pathways for the 40S precursor harboring the 20S pre-rRNA and the 60S precursor associated with the $27SA_2$ pre-rRNA (Fig. 1A; Supplemental Fig. S1A; Cheng et al.

2020). Recently, it was shown that also pre-60S specific factors (Noc2, Noc1, Brx1) are bound already cotranscriptionally to form a very early pre-60S particle (Supplemental Fig. S1A; Sanghai et al. 2023).

The $27SA_2$ pre-rRNA is further processed in the nucleolus in an elaborated manner to form the mature 5′ end of the 5.8S rRNA. On the main route, RNase MRP in the first step cleaves at site A3 forming the $27SA_3$ pre-rRNA (Lygerou et al. 1996; Esakova et al. 2013). Trimming of the $27SA_3$ pre-rRNA by Rrp17 or Rat1 to the B_S site generates one mature 5′ end of the 5.8S rRNA (Henry et al. 1994; Oeffinger et al. 2009; Granneman et al. 2011). A minority of the $27SA_2$ pre-rRNA is directly cleaved by an unknown factor at site B_L forming a slightly longer variant of the 5.8S rRNA (Fig. 1A; Faber et al. 2006).

The 27SB pre-rRNA already shows the mature 5′ end of the 5.8S rRNA and the mature 3′ end of the 25S rRNA, but requires the removal of the ITS2 to finalize maturation (Gasse et al. 2015). The ITS2 region forms a distinct structural feature of pre-60S particles called the "foot," with the C2 site being exposed to be cleaved by the heterotetrameric Las1–Grc3 complex (Castle et al. 2013; Wu et al. 2016; Pillon et al. 2019, 2020). Subsequently, coordinated 5′–3′ and 3′–5′ trimming events also result in the dissociation of the foot structure-associated proteins (Gasse et al. 2015; Fromm et al. 2017). The 5′–3′ exonucleases Rat1 and Rrp17 form the mature 5′ end (site C1) of the 25S RNA (Fig. 1A; Geerlings et al. 2000; Oeffinger et al. 2009). The mature 3′ end (site E) of the 5.8S rRNA is formed by stepwise 3′–5′ trimming by the exosome, Rex1, Rex2, and Ngl2 (Fig. 1A; Mitchell et al. 1997; Briggs et al. 1998; van Hoof et al. 2000; Dziembowski et al. 2007; Thomson and Tollervey 2010; Schuller et al. 2018).

Several black boxes in the processing of the 35S pre-rRNA into mature rRNAs remain (Fig. 1A, question marks). Therefore, finding of yet unknown nucleases requires a reliable technique to analyze pre-rRNA. Furthermore, drugs that inhibit ribosome biogenesis come into the focus of medical research as they are expected to have high potential in antitumor chemotherapy (Awad et al. 2019; for review, see Catez et al. 2019; Zisi et al. 2022). An obstruction for this research is the lack of a simple screening procedure to identify specific ribosome biogenesis inhibitors. As substances that interfere with ribosome formation often result in the accumulation of rRNA precursors or the formation of aberrant processing intermediates (e.g., 23S pre-rRNA), a simple method to monitor processing defects will facilitate the characterization of potential inhibitors.

To date two elaborative approaches are commonly used to investigate pre-rRNA species: northern blotting and primer extension. For northern blots, the separation of RNA in agarose gels with subsequent transfer to a membrane allows the detection of different RNA species with specific radioactive labeled probes (Supplemental Figs. S1B and S2A; for protocols, see Kevil et al. 1997; Streit et al. 2009). The biggest advantage of this widely used method is that the RNA is unamplified and can, therefore, be evaluated not only qualitatively but also quantitatively. However, this method is time-consuming and cannot discriminate some processing intermediates as their length cannot be precisely determined.

To overcome the limitation of precise size estimation with northern blots, they are often combined with primer extension experiments. With a primer binding near the region of interest, the reverse transcriptase amplifies the sequence in the 5′ direction. Also here, radioactive labeling is used to detect the reverse transcription termination at the ends of an rRNA processing intermediate (Venema et al. 1998; Carey et al. 2013). The resulting cDNA fragments are separated in polyacrylamide gels to provide single-nucleotide resolution.

We aimed to evolve primer extension to simplify the detection of pre-rRNA species without the use of radioactivity. In our workflow, an RNA linker is ligated either to the 5′ or 3′ end of the RNA before reverse transcription and PCR amplification (Fig. 1B). The workflow is similar to 5′ and 3′ RACE but uses rRNA-specific probes for the primer extension reaction (Frohman et al. 1988). The method described here allows reliable discrimination of pre-rRNA species from whole cell lysates, as well as purified pre-ribosomes using only minute amounts of RNA. As demonstrated by the characterization of a novel aberrant RNA accumulating upon LiCl-promoted nuclease inhibition, it enables simple and unambiguous identification of hitherto unknown RNAs.

RESULTS

Riboprobing as a new tool to investigate rRNA maturation

To simplify the characterization of different pre-rRNA species we aimed to develop a nonradioactive workflow for fast identification of a broad spectrum of precursor rRNAs. The protocol involves RNA-linker ligation to (pre-) rRNA, reverse transcription, and subsequent PCR amplification (Fig. 1B), allowing signal detection with standard laboratory equipment. We designed the RNA linkers in a way to prevent cofold structure formation with the rRNA and to ligate to either the 5′ or the 3′ end of the pre-rRNAs. For this purpose, the 5′ linker lacks a 5′ phosphate and thus only allows 3′OH (linker) to 5′P (rRNA) ligation. The 3′ linker was designed with a 3′ cap (23ddC) disabling ligation to any 5′P of RNA, but with a 5′P to ligate to 3′OH of different rRNA ends.

To investigate the 5′ ends of different pre-rRNAs, oligonucleotide probes also used for northern blots can be used to prime reverse transcription (Supplemental Fig. S2A). Analysis of all 3′ ends using a single primer for reverse transcription, binding to the 3′ RNA linker, is possible. For

visualization, cDNAs are amplified via PCR. As the binding site of the primers to the cDNA is known, the resulting products can be identified according to their length when separated on an agarose gel (Supplemental Fig. S2B). Even though separation on agarose gels does not have a per-nucleotide resolution, Sanger sequencing allows to pinpoint the end of a processing intermediate, as the linker sequence is part of the sequencing reaction. During method development we sequenced all visualized products, but this is not needed once a linker–primer pair is established. An advantage of Riboprobing in comparison to primer extension is that the probability of signals derived from unspecific reverse transcription runoff (e.g., due to base modifications) is low and would be identified via Sanger sequencing.

Minute amounts of RNA can be used to discriminate 27S pre-rRNA species

Initially, we wanted to discriminate the three different 27S pre-rRNA species, $27SA_2$, $27SA_3$, and 27SB, as this is not possible by northern blots (Fig. 2E). In the first step, we tested what amount and type of RNA isolates can be used in our Riboprobing workflow. RNA was either isolated from intact yeast cells, crude extract, or from pull-downs of pre-ribosomes (Fig. 2A). We took the low concentration of RNA in pull-downs of pre-ribosomes as a reference value and diluted the total and crude extract RNA to the same concentration. Further, we included a 10 times more diluted and 2.5 times less diluted sample to determine the ideal RNA concentration for the experiment (Fig. 2B). cDNA was synthesized using the C_1C_2 probe and subsequently amplified with the 5′ linker primer and the C_1C_2 probe (Fig. 2C). This primer was selected for cDNA synthesis as it only amplifies 27S pre-rRNA species but no 7S pre-rRNA or mature rRNAs.

We observed a strong band of 400-nt length in all samples indicating that we amplified 27SB pre-rRNA from total RNA as well as crude extract and pull-down RNA isolates independent of the RNA concentration used (Fig. 2B). Both concentrations of Noc2-TAP coisolated RNA led to one additional 550-nt band originating from the $27SA_2$ pre-rRNA. Detection of $27SA_2$ and 27SB pre-rRNA in RNA isolated from Noc2-TAP pull-downs fit to data obtained by northern blotting (Supplemental Fig. S3D). The band originating from the $27SA_2$ pre-rRNA was also observed in the tested samples from total cell RNA isolates. With crude extract RNA, at least 200 ng of RNA was used for linker ligation to allow reliable detection of $27SA_2$ pre-rRNA (Fig. 2B). This indicates that the ratio of $27SA_2$ to 27SB pre-rRNA in crude extract samples is lower than in total RNA isolates, which was confirmed by quantification of the northern blot signals for $27SA_2$ to the $27S_{total}$ pre-rRNA (Fig. 2D,E). For further experiments, we used at least 200 ng of RNA when samples were derived from total cell RNA extracts or crude extract isolates, but only 20 ng when RNA from pre-ribosomal particle pull-downs was tested.

When using total cell or crude extract RNA, we observed additional, less intense bands (Fig. 2B). Addition of RNase A to the cDNA samples had no effect on these bands, indicating that they arose from amplified cDNA and not from remaining RNA (Supplemental Fig. S3A). Raising the annealing temperature during PCR did not eliminate the unspecific products (Supplemental Fig. S3A). Some of these bands even appeared faintly when the reverse transcription reaction was performed without any primer, suggesting self-priming by stem structures in the rRNA (Supplemental Fig. S3B). We did not detect such unspecific bands in other linker–primer combinations (Fig. 3). Therefore, the amplification of these self-priming stem structures occurs through the binding of the C_1C_2 primer to degenerate sites (Supplemental Fig. S3B). Sequencing revealed that the unspecific 800- and 380-nt PCR products start around nucleotide 380 in the 25S rRNA, amplifying the 5′ region of $27SA_2$ pre-rRNA up to site A2 (800 nt) or mature 25S rRNA to site C1 (380 nt) (Supplemental Fig. S3C; Supplemental Information, Sequences 1 and 2). The 200-nt-long fragment starts at the 3′ end of the 5.8S rRNA amplifying mature 5.8S rRNA in the 5′ direction (Supplemental Fig. S3C; Supplemental Information, Sequence 3). Tested in silico the C_1C_2 primer sequence indeed partly aligns to those regions in the mature 25S and 5.8S rRNA sequences. This mismatch might, therefore, explain the observed unspecific products. Still, unambiguous detection of the 27S pre-rRNA species in total RNA extracts was possible (Fig. 2B).

RNA isolated from intact cells and crude extracts contains a very high proportion of mature rRNAs compared to RNA coisolated from purified pre-ribosomes. Therefore, the appearance of unspecific fragments amplified from mature rRNAs is more likely in such complex samples. Still, the bands of interest (27S pre-rRNA species) could easily be distinguished and identified because of their different length.

Riboprobing allows the detection of various pre-rRNA processing intermediates

As we were able to discriminate $27SA_2$ and 27SB pre-rRNA by Riboprobing, we applied the workflow also to other pre-rRNA processing intermediates. Tandem affinity purifications with different bait proteins were performed to isolate pre-ribosomes containing different pre-rRNA species (Fig. 3C). To confirm successful purification, the protein composition of pre-ribosomes was confirmed by western blotting (Fig. 3A) and Coomassie staining (Supplemental Fig. S4B) and the copurified pre-rRNA species were analyzed by northern blotting (Fig. 3B). Before cDNA amplification with different primer pairs, either the 5′ linker or the 3′ linker was ligated to the RNA isolated from purified pre-ribosomes (Fig. 3D–G).

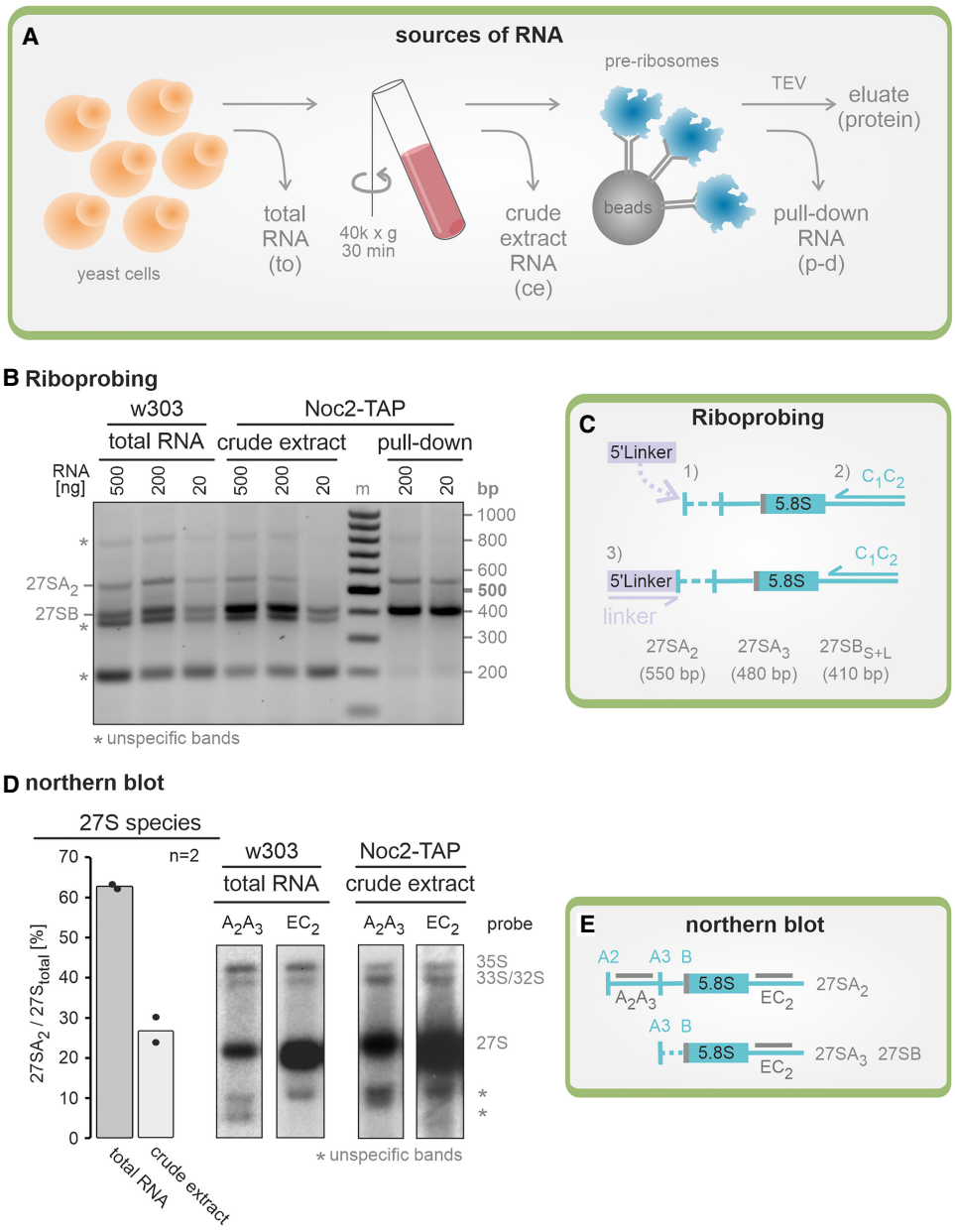

FIGURE 2. Small amounts of different RNA isolates allow discrimination of 27S pre-rRNA species. (*A*) Different sources for RNA isolation were tested with the Riboprobing workflow: total cellular RNA, RNA from crude extracts, and RNA from pre-ribosome pull-downs. (*B*) 1.5% agarose gel separating the products of the Riboprobing workflow. Different initial RNA amounts were analyzed by Riboprobing. For pull-down samples, 20 ng of RNA was used, whereas total RNA and crude extract RNA samples required at least 200 ng for a reliable detection of $27SA_2$ and 27SB pre-rRNA. (m) 100-bp ladder (Thermo Fisher). (*C*) Riboprobing workflow scheme for *B* with the expected length of the different 27S pre-rRNA species. (*D*) Comparison of $27S_{total}$ (detected by EC_2 probe) to $27SA_2$ (detected by A_2A_3 probe) pre-rRNA signals in total RNA and crude extract RNA samples. The X-ray films were exposed to show roughly the same intensities for the 35S/32S pre-rRNA. After quantification of the signals and normalizing the 27S pre-rRNA species to the 35S pre-rRNA, the proportion of $27SA_2$ pre-rRNA in the $27S_{total}$ pre-rRNA was calculated and expressed in %. (*E*) Binding positions of probes used for 27S pre-rRNA species detection by northern blotting.

RNA isolated from 90S pre-ribosomal particles purified via Utp14-TAP was investigated with an 18S primer and the 5′ linker, which resulted in two PCR products. Because of the length and confirmed by Sanger sequencing, the 5′ linker was ligated to site A1 (220 nt) and site A0 (310 nt) reflecting the mature 5′ end of the 18S rRNA (A1) and the 33S pre-rRNA (A0), respectively (Fig. 3D; Supplemental Information, Sequences 4 and 5). Using the same linker–primer combination with RNA isolated from pre-40S particles purified with Tsr1-TAP as bait protein only led to a signal for the mature 5′ end of the 18S rRNA as expected (Fig. 3B,D).

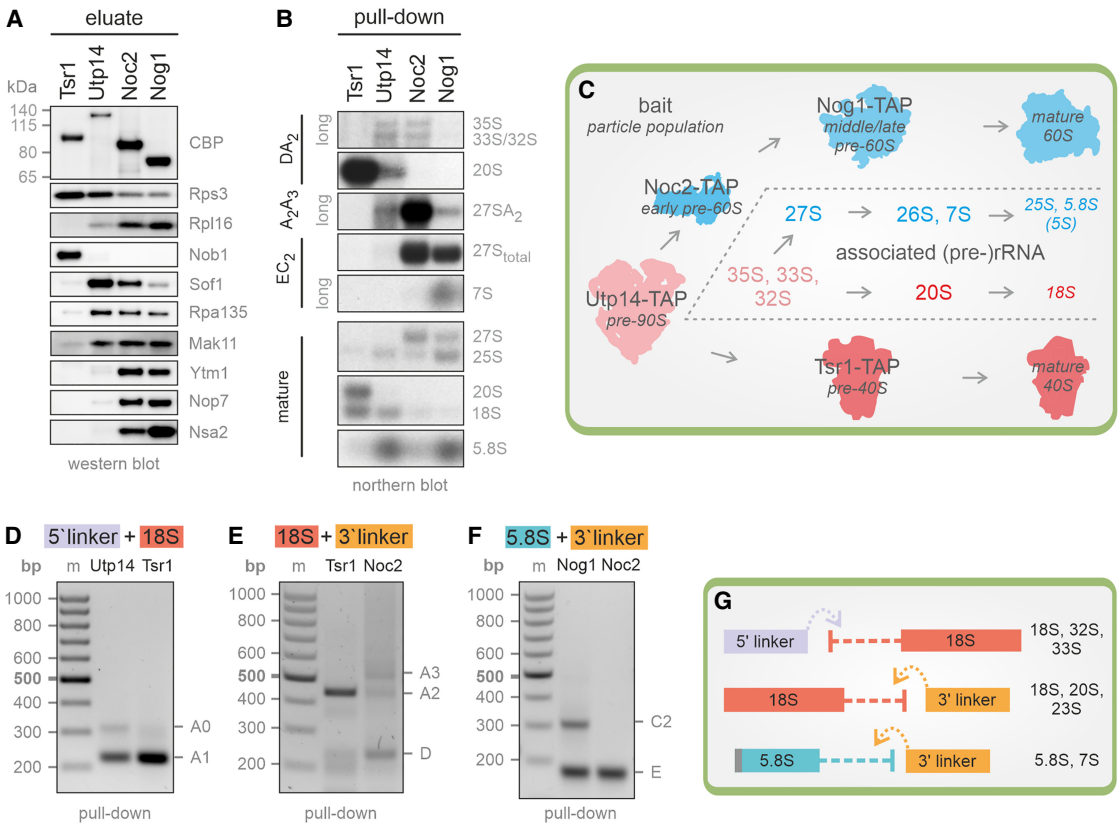

FIGURE 3. Detection of various pre-rRNA processing intermediates by combining different linkers and primers. (*A*) Western blot of TAP purification eluates with different bait proteins as labeled. Antibodies used for the detection of assembly factors or ribosomal proteins are indicated at the *right* side. (*B*) Northern blot of RNA isolated from different pre-ribosome pull-down samples. The probes used are indicated on the *left*, (pre)-rRNA species on the *right*. (*C*) Simplified scheme to show at which stages the bait proteins used are involved in ribosome biogenesis. The copurifying pre-rRNA species are also indicated. (Light pink) 90S pre-ribosomal particle/pre-rRNA, (soft blue) 60S pre-ribosomal particle/pre-rRNA, (soft red) 40S pre-ribosomal particle/pre-rRNA. (*D–F*) 1.5% agarose gel separating the products of the Riboprobing workflow. (m) 100-bp ladder (Thermo Fisher). (*D*) RNA, isolated from Utp14-TAP and Tsr1-TAP pull-downs, was ligated with the 5′ linker and after cDNA synthesis amplified with 5′ linker and 18S primer. (*E*) RNA, isolated from Tsr1-TAP and Noc2-TAP pull-downs, was ligated with the 3′ linker and after cDNA synthesis amplified with the 18S primer and 3′ linker. (*F*) RNA, isolated from Nog1-TAP and Noc2-TAP pull-downs, was ligated with the 3′ linker and after cDNA synthesis amplified with the 5.8S primer and 3′ linker. (*G*) Riboprobing workflow used in *D–F* with detectable pre-rRNA species.

The RNA in the pre-40S Tsr1-TAP pull-down was also investigated using the 3′ linker in combination with an 18S primer. The 400-nt band arises from 3′ linker ligation to site A2, showing that the 3′ end of 20S pre-rRNA was amplified (Fig. 3E; Supplemental Information, Sequence 6). We chose the Noc2-TAP pull-down to isolate RNA from early pre-60S particles as a control, which should not amplify a product for the pre-40S specific 20S pre-rRNA. Very weak bands at 500 nt originating from 23S pre-rRNA (linker ligation to site A3), 400 nt (20S pre-rRNA), and 250 nt originating from 18S rRNA (linker ligation to site D) were detected (Fig. 3E; Supplemental Information, Sequences 7 and 8). Weak signals for those (pre-)rRNAs were also visible in the northern blots (Supplemental Fig. S4C).

Although Noc2-TAP was used to isolate early nucleolar, $27SA_2$, and 27SB pre-rRNA containing pre-ribosomes (Fig. 2), Nog1-TAP was used to isolate later pre-60S particles (Fig. 3A,B). RNA isolated from Nog1-TAP pull-downs was investigated by combining the 3′ linker with a primer binding to the 5.8S rRNA. Two bands, one at 300 nt (linker ligation to site C2 of the 7S pre-rRNA) and one at 150 nt (linker ligation to mature 3′ end of the 5.8S rRNA) were resolved (Fig. 3F; Supplemental Information, Sequences 9 and 10). RNA isolated from Noc2-TAP pull-downs only led to a signal for mature 5.8S rRNA, a carryover of mature rRNAs during the purification process (Fig. 3B).

We also investigated RNA isolated from intact cells with the same combinations of 3′ or 5′ linker and different primers. Although the 5′ linker in combination with the 18S primer only amplified mature rRNA, we could detect 20S pre-rRNA (3′ linker and 18S primer) and a weak signal for 7S pre-rRNA (3′ linker and 5.8S primer) (Supplemental Fig. S4A). Most likely the preponderance of mature rRNA captured the 18S primer, disabling sufficient detection of the short-lived 33S pre-rRNA (Supplemental Fig. S4A).

Depletion of Rlp7 leads to accumulation of $27SA_3$ pre-rRNA, but cleavage by RNase MRP is prevented by LiCl

We did not detect the low abundant $27SA_3$ pre-rRNA in any sample, even if they harbored the ancestor ($27SA_2$) and descendant (27SB) pre-rRNAs (Fig. 2). To verify whether our protocol allowed detection of this pre-RNA, we depleted the ribosome assembly factor Rlp7, a condition that was shown to lead to $27SA_3$ pre-rRNA accumulation (Dunbar et al. 2000; Sahasranaman et al. 2011). Indeed, when Rlp7 was depleted for 16 h, Riboprobing with the 5′ linker and C_1C_2 primer resulted in an additional band of 460 nt length in the total cell RNA sample (Fig. 4A). Sanger sequencing confirmed that this product was derived from $27SA_3$ pre-rRNA, whereas the 540-nt product arose from $27SA_2$ pre-rRNA (Fig. 4A). Sanger sequencing of the 400-nt-long amplification product led to overlapping sequencing signals due to the two ends of 27SB pre-rRNA ($27SB_L$ and $27SB_S$) differing in only 6 nt (Supplemental Information, Sequences 11–13). In the case of depleted Rlp7, the main form should be $27SB_L$ pre-rRNA, as $27SB_S$ pre-rRNA is formed from $27SA_3$ pre-rRNA (Fig. 1A; Dunbar et al. 2000). With agarose gel electrophoresis we could not resolve such little differences, but still the sequencing chromatogram allowed us to argue that the main form might be $27SB_L$ pre-rRNA (Fig. 4A). Northern blot analysis of the Rlp7-depleted strain showed minute levels of 7S and 20S pre-rRNAs and 25S rRNA. Levels of $27S_{total}$ and $27SA_2$ pre-rRNA decreased, whereas levels of 35S pre-rRNA increased. We also detected a weak 23S pre-rRNA signal (Fig. 4D). The appearance of 23S pre-rRNA was also seen with Riboprobing when total cell RNA was analyzed using the 3′ linker and 18S primer (Supplemental Fig. S5A).

To test how inhibition of cellular RNases interferes with pre-rRNA processing we treated cells additionally with lithium chloride (LiCl), which was described to directly inhibit the RNase MRP endonuclease and indirectly also the 5′–3′ exonucleases Rat1 and Xrn1 (Dichtl et al. 1997). Therefore, we combined 16 h depletion of Rlp7 with LiCl treatment for 3 h before cell harvesting (Fig. 4C). In contrast to the sample without LiCl treatment, a strong signal for $27SA_2$ pre-rRNA but no $27SA_3$ pre-rRNA and hardly any 27SB pre-rRNA signals were detected by Riboprobing (Fig. 4B). This was confirmed by northern blotting showing an accumulation of $27SA_2$ pre-rRNA compared to Rlp7 depletion alone. These results are in line with the published inhibition of RNase MRP by LiCl, as the $27SA_2$ pre-rRNA cannot be processed to $27SA_3$ pre-rRNA (Fig. 1A; Dichtl et al. 1997). Further, northern blotting revealed a strong 32S pre-rRNA signal and also an accumulation of 20S pre-rRNA compared to Rlp7 depletion alone (Fig. 4D).

As the signal intensities for the different 27S pre-rRNA species changed in a similar manner in Riboprobing and northern blotting results (Fig. 4B,D), we quantified the signals for both experimental approaches (see Materials and Methods). As shown in Figure 4E, the ratio of the $27SA_2$ pre-rRNA signal to the total 27S pre-rRNA signal showed a good agreement between Riboprobing and northern blotting.

LiCl treatment for 3 h in wild-type conditions drastically changed the pre-rRNA content, leading to strongly decreased levels of nearly all pre-rRNA species. As the 35S pre-rRNA was also reduced, LiCl treatment might also affect Pol I transcription (Fig. 4D). With northern blotting, only 20S pre-rRNA, minor amounts of 24S pre-rRNA, and a band migrating above the 20S pre-rRNA that we from now on refer to as 22SE (see Discussion) were detected (Fig. 4D; Supplemental Fig. S5B). Riboprobing with the 5′ linker and C_1C_2 primer identified no signal for $27SA_2$ and $27SA_3$ pre-rRNA and only a very weak 27SB pre-rRNA signal (Fig. 4B).

$27SA_3$ pre-rRNA coisolated with Noc2-TAP particles is turned over during purification

To analyze if the $27SA_3$ and 22SE pre-rRNA species are part of a pre-ribosomal particle, Noc2-TAP was chosen as the bait protein as it is present in very early pre-ribosomal particles (Fig. 3B). Upon depletion of Rlp7, the Noc2-TAP particle shifted to a very early form of pre-60S particle, as previously described (Fig. 5B; Supplemental Fig. S6A; Sahasranaman et al. 2011). Very little $27SA_3$ pre-rRNA was detected in the pull-downs of these particles, compared to the total RNA samples (Figs. 4A and 5C). To test, whether $27SA_3$ pre-rRNA precipitates during the purification procedure, we analyzed the insoluble fraction of the cell lysate in regard to $27SA_3$ pre-rRNA levels, but hardly any signal was detected in the pellet (Supplemental Fig. S6B). Next, we added ribonucleoside vanadyl complex (RVC) to the cell lysate, a substance that protects RNA ends from degradation. Indeed, we detected a more prominent signal for $27SA_3$ pre-rRNA in the presence of RVC, suggesting that during purification unprotected RNA ends were degraded (Fig. 5C). Unfortunately, this substance seems to interfere with TEV cleavage as no particles were recovered in the TEV eluate (Fig. 5A).

Moreover, we tested the effect of LiCl treatment in combination with the Rlp7 depletion on the pre-rRNA composition of Noc2-TAP particles (Fig. 5B,C). The $27SA_3$ pre-rRNA was shifted to the earlier $27SA_2$ pre-rRNA and 33S/32S pre-rRNA copurified with Noc2-TAP pull-downs.

Lithium chloride treatment accumulates an undescribed aberrant processing intermediate

After LiCl treatment of the nondepleted P_{GAL1}-Rlp7 strain, Noc2-TAP copurified a clearly altered set of pre-rRNAs and proteins compared to the untreated strain (Fig. 5A,B; Supplemental Fig. S6A,C). Besides minor levels of 27SB

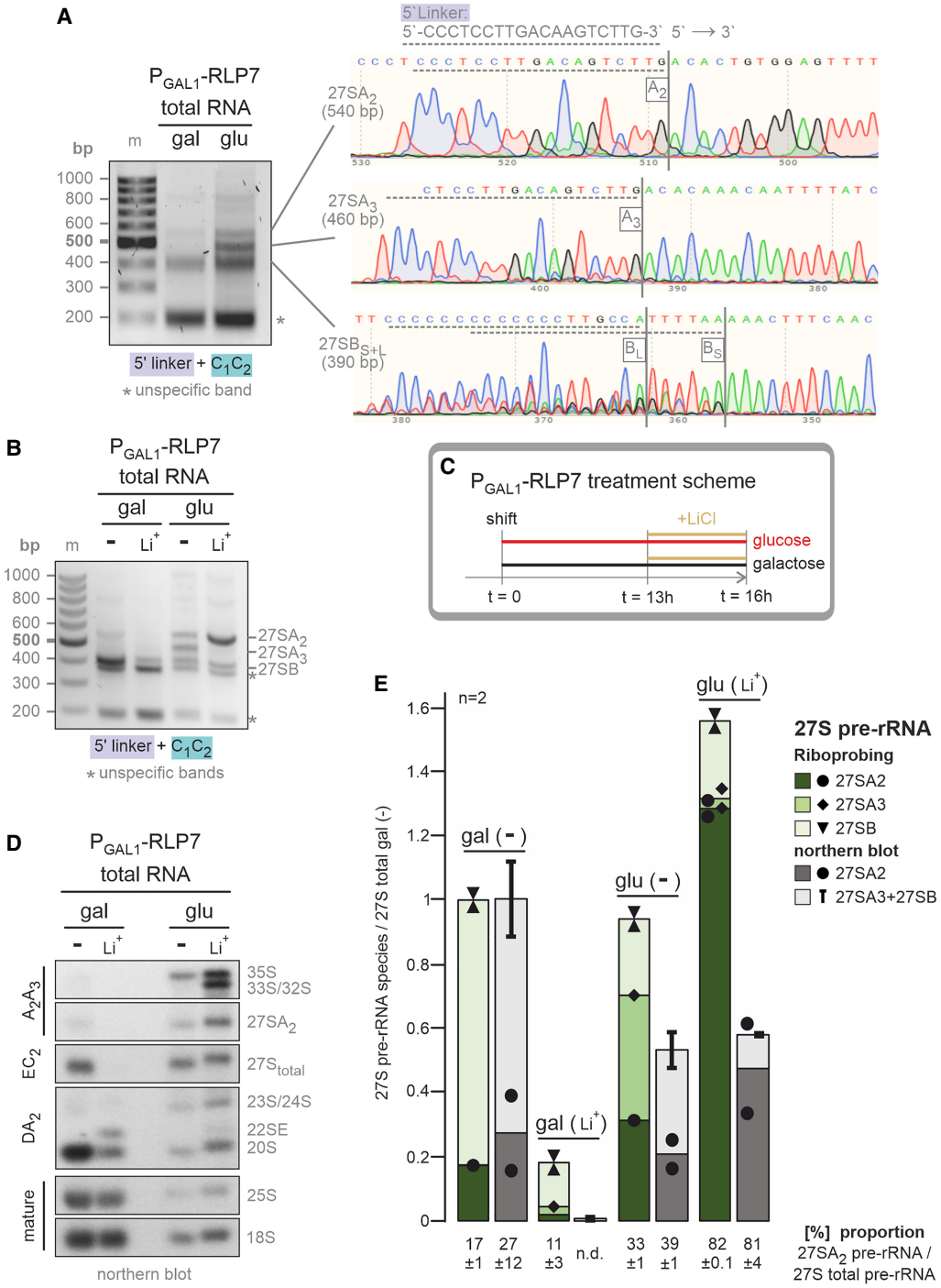

FIGURE 4. Depletion of Rlp7 leads to the accumulation of $27SA_3$ pre-rRNA, which is shifted to $27SA_2$ pre-rRNA after nuclease inhibition by lithium chloride treatment. The P_{GAL1}-Rlp7 strain was grown in galactose-containing medium (wild-type condition; gal) or incubated in glucose-containing medium for 16 h (Rlp7 depleted; glu). Additionally, both conditions were combined with lithium chloride treatment for 3 h (Li^+). (–) Untreated samples. (*A*,*B*) 1.5% agarose gel separating the products of the Riboprobing workflow. (m) 100-bp ladder (Thermo Fisher). (*A*) Depletion of Rlp7 for 16 h resulted in a band with 460 nt length that was confirmed to arise from $27SA_3$ pre-rRNA by Sanger sequencing. 27SB pre-rRNA has two forms that can be detected in the overlapping sequencing results. (*B*) Although depletion of Rlp7 led to $27SA_3$ pre-rRNA accumulation, additional treatment with lithium chloride led to a strong signal arising from the earlier $27SA_2$ pre-rRNA. (*C*) Treatment scheme for the P_{GAL1}-Rlp7 strain. (*D*) Northern blot of the P_{GAL1}-Rlp7 strain grown in galactose or glucose-containing medium and treated with LiCl. An untreated culture served as control. Probes indicated on the *left*; (pre)-rRNA species on the *right*. (*E*) The different 27S pre-rRNA species were quantified using either signals from the northern blot (see Fig. 4C) or signals from the Riboprobing experiment (see Fig. 4B). For all conditions in each experimental approach, we normalized the signal intensities to the total 27S pre-rRNA signal in the untreated wild-type strain grown in galactose-containing media. The mean values of two biological replicates are shown.

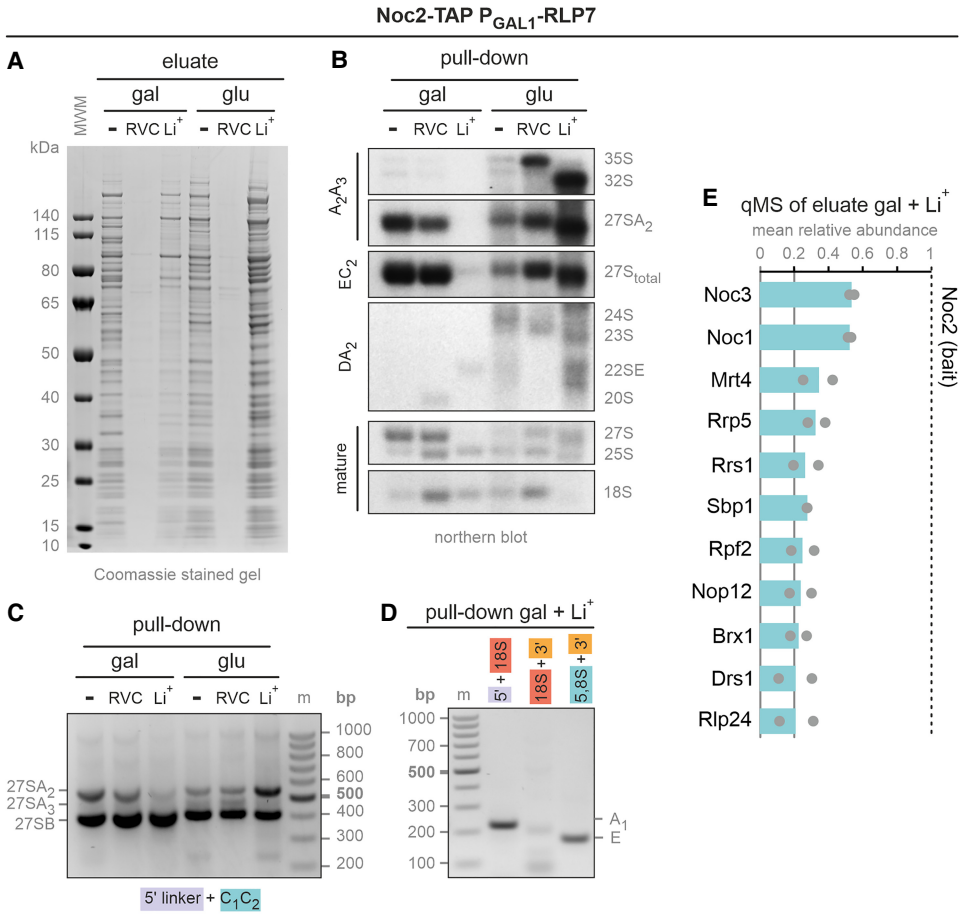

FIGURE 5. The 27SA$_3$ pre-rRNA copurifies with Noc2-TAP when Rlp7 is depleted, but is degraded during purification. Pre-ribosomal particles were purified from the *P$_{GAL1}$*-Rlp7 strain using Noc2-TAP as bait protein. The strain was grown in a galactose-containing medium (wild-type conditions; gal) or incubated in a glucose-containing medium for 16 h (Rlp7 depleted; glu). Additionally, cells were treated with lithium chloride for 3 h (Li$^+$) or RVC was added during purification. (–) Untreated samples. (*A*) Coomassie-stained gel with TEV eluates of Noc2-TAP particles from the Rlp7 depleted (glu) or control strains (gal). (MWM) PageRuler prestained protein ladder (Thermo Fisher). (*B*) Northern blot of RNA isolated from the *P$_{GAL1}$*-Rlp7 strain by Noc2-TAP pull-downs. Probes indicated on the *left*; (pre)-rRNA species indicated on the *right*. (*C*,*D*) 1.5% agarose gel separating the products of the Riboprobing workflow. (m) 100-bp ladder (Thermo Fisher). (*C*) Riboprobing using 5′ linker and C$_1$C$_2$ primer and RNA isolated from the Noc2-TAP pull-downs after Rlp7 depletion (glu). Riboprobing with RNA isolated from the same strain grown in galactose-containing medium (gal) served as a control. (*D*) RNA isolated from Noc2-TAP pull-downs of the *P$_{GAL1}$*-Rlp7 strain grown in galactose-containing medium and treated with LiCl was investigated by Riboprobing using the indicated combinations of linker and primer. (*E*) Assembly factors strongly coenriched with the Noc2-TAP bait protein in pull-downs from the LiCl-treated strain were identified by qMS. Relative abundance to the Noc2 bait protein was calculated. The mean abundance of assembly factors with a standard deviation of <0.1 and an abundance of >0.2 relative to the bait protein are shown (dots represent individual replicates).

pre-rRNA, we also observed 22SE pre-rRNA to be pulled down (see Discussion; Figs. 5B and 4D). Northern blot analysis indicated that this fragment contained both, 18S and 5.8S rRNA (Supplemental Figs. S5C and S4B), which was confirmed by Riboprobing using different combinations of 3′ and 5′ linkers and primers and Sanger sequencing (Fig. 5D). The sequencing showed that this fragment spans from the mature 5′ end of the 18S rRNA to the mature 3′ end of the 5.8S rRNA.

We also detected a drastic reduction of Noc2-TAP copurifying proteins upon LiCl treatment (Fig. 5A). For a better characterization of this Noc2-RNP, qMS was performed and the TOP3 stoichiometry relative to the bait abundances was calculated for 121 copurifying proteins (Supplemental Excel Sheet S1; see Materials and Methods; Silva et al. 2006; Fabre et al. 2014). Next, we included proteins with an abundance of at least 0.2 (20%) relative to the bait, but excluded all proteins in this group if the standard deviation between replicates was >0.1. According to this analysis 11 assembly factors and several r-proteins were pulled down with Noc2-TAP after LiCl treatment (Fig. 5E; Supplemental Fig. S7). The two assembly factors with the highest relative abundance were Noc1 and Noc3 (~50% relative to the Noc2 bait protein); both also gave pronounced signals in the western blot (Supplemental Fig. S6A). Although other pre-60S assembly factors were also found in the qMS

analysis, 90S pre-ribosomal assembly factors were absent, which was unexpected for a fragment that includes the full 18S rRNA sequence. In line with this result, the most abundant r-proteins detected were from the large ribosomal subunit and not from the small ribosomal subunit (Supplemental Fig. S7).

DISCUSSION

Riboprobing allows reliable detection of pre-rRNA species

We developed and evaluated a new workflow to detect and identify different pre-rRNA species and to pinpoint their exact 5′ and 3′ ends. Similar to 5′ and 3′ RACE, Riboprobing depends on the ligation of RNA linkers to either 5′ or 3′ RNA ends but uses (pre-)rRNA-specific primers for subsequent PCR amplification (Fig. 1B; Frohman et al. 1988). The method requires small amounts of RNA and is sensitive enough to detect even low abundant pre-rRNAs in total cell RNA samples, crude extracts as well as purified pre-ribosomes (Figs. 2–5). The amplification products can be Sanger-sequenced to unambiguously identify processing intermediates, as the site of the linker ligation defines the pre-rRNA end. Because the ligation efficiency of RNA ligases can be influenced by secondary structures near the ligation site (Zhuang et al. 2012; Fuchs et al. 2015), which could influence the signal intensity, we compared the results from Riboprobing and northern blotting (Fig. 4E). Both methods detected a similar ratio of $27SA_2$ pre-rRNA to a total of 27S pre-rRNA, indicating that Riboprobing allows semiquantitative analysis.

The workflow presented here will be especially useful if large sample sets should be screened for the accumulation of specific pre-rRNA processing intermediates in total RNA extracts (e.g., $27SA_3$ or 23S pre-rRNA). Northern blots allow a global, quantitative (pre-)rRNA analysis, but Riboprobing could replace primer extension, when specific pre-rRNA species are of great interest. Although we developed the workflow using RNA isolates from yeast, it could also be applied to isolated RNA samples from other organisms by choosing appropriate primers.

Fast turnover of $27SA_3$ pre-rRNA keeps early pre-rRNA processing running

Depletion of so-called A3 factors was described previously to lead to $27SA_3$ pre-rRNA accumulation in total cell extracts (Sahasranaman et al. 2011). However, this pre-rRNA was only detected in pre-ribosomal pull-downs after depletion of the 5′–3′ exonucleases Rat1 and Xrn1 (Sahasranaman et al. 2011). In line with this, we only detected $27SA_3$ pre-rRNA in pull-downs when the pre-rRNA ends were protected from 5′ to 3′ exonucleolytic degradation by adding the RVC ribonuclease inhibitor (compare Figs. 4B and 5C).

Our data and those in the literature show that a block in $27SA_3$ pre-rRNA processing (and thus a $27SA_3$ pre-rRNA accumulation) also leads to massive 35S pre-rRNA accumulation, suggesting a feedback loop that prevents processing at site A0 (Fig. 6A; Supplemental Fig. S8A). This could serve as a quality control step to signal perturbations in the pathway to earlier stages of ribosome biogenesis. In contrast, additional LiCl treatment causes pronounced accumulation of $27SA_2$ pre-rRNA and results in increased levels of 32S and 33S pre-rRNAs (Figs. 4–6A; Supplemental Fig. S8A). This difference is likely caused by trapping different assembly factors on the accumulating pre-rRNA species, which leads to their shortage in earlier assembly steps. As both very early pre-60S and late 90S pre-ribosomal particles accumulate, all Noc2 might be captured at those stages and therefore be missing on newly synthesized 35S pre-rRNA, explaining why this precursor accumulates in total RNA extracts but not in Noc2 pull-downs (Figs. 4–6A; Supplemental Fig. S8A).

22SE is a new aberrant pre-rRNA species associated with a small Noc2-RNP

Under nondepleted conditions, pre-rRNA processing was severely affected upon LiCl treatment. The only pre-rRNAs detected in the total cell extracts were 24S pre-rRNA, 20S pre-rRNA, and the newly discovered 22SE pre-rRNA. The length of this intermediate lies between the previously described aberrant 22S and 22.5S processing intermediates, which prompted us to designate it 22SE pre-rRNA (as it reaches to site E; Supplemental Fig. S8B).

When assembly factors of the 90S pre-ribosome are defective, aberrant 23S/22.5S pre-rRNA (5′ end to site A3/A2), 22S/21.5S pre-rRNA (site A0 to site A3/A2) and/or 21S pre-rRNA (site A1 to site A3) accumulate, which were proposed to be processed to 20S pre-rRNA (site A1 to site A2) (Fig. 6B, A2 and A3 pathway; Allmang et al. 2000; Fatica et al. 2003; Bernstein et al. 2004; Delprato et al. 2014; Boissier et al. 2017; Dielforder et al. 2022). In contrast, mutations affecting RNase MRP activity cause accumulation of aberrant 24S pre-rRNA (reaching from the 5′ end of the 35S rRNA to site E), in which processing in 5′ETS and ITS1 was completely blocked and no (pre-)rRNA downstream from 5.8S rRNA (ITS2, 25S rRNA, and 3′ETS) was detected (Lindahl et al. 2009; Li et al. 2021). Very recently this 24S pre-rRNA was also described to sediment with a small RNP rather than 60S or 90S pre-ribosomes (Li et al. 2021).

Consistent with its known inhibitory effect, LiCl treatment showed a similar processing defect as that described for mutations in the genes coding for the RNase MRP (Dichtl et al. 1997). We propose that the 24S pre-rRNA is processed at sites A0 and A1, producing the 22SE pre-rRNA described here (Fig. 6B). However, LiCl might additionally also inhibit Pol I, because only very little 35S pre-rRNA was detected in the treated strain.

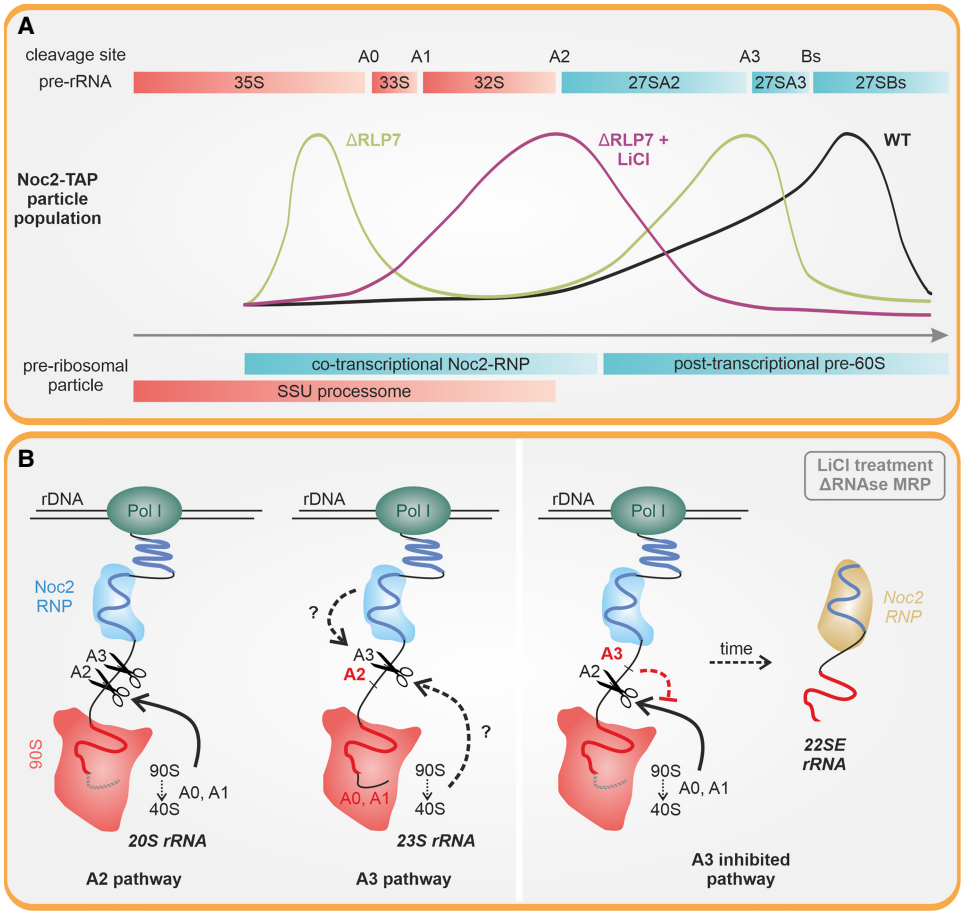

FIGURE 6. Shift of the Noc2-TAP particle populations upon Rlp7 depletion and treatment with LiCl. (*A*) Scheme depicting how the population of Noc2 containing pre-ribosomal particles (WT: wild-type conditions, black line) is shifted to earlier stages either due to depletion of Rlp7 (ΔRlp7, green line) or a combination of Rlp7 depletion and LiCl treatment (ΔRlp7 + LiCl, purple line) (Fig. 5). (*B*) Under wild-type conditions, pre-rRNA is processed in the order A0 → A1 → A2 → A3 (A2 pathway) leading to a pre-40S subunit associated with 20S pre-rRNA. Perturbations in the first pre-rRNA processing steps cause the cells to switch to the A3 pathway, which allows cleavage at site A3 before the other processing steps (A3 pathway), resulting in a pre-40S subunit associated with 23S pre-rRNA (and its downstream processing intermediates; Supplemental Fig. S8B). A block in processing at site A3 triggers a feedback loop that prevents processing at site A2, resulting in the formation of aberrant 22SE pre-rRNA (or 24S pre-rRNA if sites A0 and A1 are not processed) (Figs. 4 and 5).

The Noc2-TAP particle copurifying 22SE pre-rRNA showed only a few other associated large subunit assembly factors (Fig. 5A,E; Supplemental Fig. S6A). According to our qMS analysis, this unusually small particle contains as main components Noc2, Noc1, and Noc3 (Fig. 5E). Noc1 and Noc2 are known to form a complex associated with the very first pre-60S particle and bind around the 5′ end of the 5.8S rRNA (Hierlmeier et al. 2013; Sanghai et al. 2023). In contrast, the heterodimeric Noc2/Noc3 complex was only found in late nucleolar pre-60S particles (Milkereit et al. 2001; Mitterer et al. 2023; Vanden Broeck and Klinge 2023). However, Noc2 and Noc3 were also found at earlier nucleolar stages by a quantitative XL-MS approach (Sailer et al. 2022).

Interestingly, the small Noc2-RNP did not copurify 24S pre-rRNA (although it was present in total cell extract RNA) or any 90S pre-ribosome-specific assembly factor. This shows that the whole 18S rRNA alone is not sufficient to assemble the 90S pre-ribosome, but the 5′ETS is strictly required. As cleavage in A2 or D would release a completely naked 18S rRNA, the 22SE pre-rRNA likely represents a dead-end product without productive downstream processing. Therefore, we propose that in contrast to other well-described aberrant pre-rRNAs, that are part of the A2 or A3 pathway (Fig. 6B), the 22SE pre-rRNA species will be degraded. As an alternative processing pathway is known for yeast, bypassing site A3 cleavage with an unidentified endonuclease (Faber et al. 2006), the pronounced effect of LiCl inhibition on site A3 leading to a complete block in ribosome biogenesis is astonishing.

In any case, the feedback mechanism we investigated here (Supplemental Fig. S6A) shows that there is direct feedback from very early pre-60S particles to earlier

cotranscriptional processing steps. Still, the basis of this interconnectivity needs to be further elucidated.

MATERIALS AND METHODS

Biological resources

All yeast strains used in this study are listed in Supplemental Table S1. Chromosomal gene fusions were generated by homologous recombination with linear PCR products to transform the corresponding yeast strain as described (Longtine et al. 1998; Janke et al. 2004). All plasmids and primers used for strain construction are listed in Supplemental Table S2.

Media and growth conditions

Yeast strains were grown at 30°C in rich media (YPD) adjusted to pH 5.5. For strains with P_{GAL1} constructs, galactose was used as a carbon source in the media (YPGal). For depletion of the P_{GAL1}-Rlp7 construct, shifting to media with glucose was performed as indicated.

Tandem affinity purification

Cultivation and harvesting

To purify pre-ribosomal particles of distinct maturation stages, yeast cells expressing C-terminal TAP-tag fusions of the assembly factors Tsr1, Utp14, Noc2, and Nog1 were grown in 2 L of YPD to a late logarithmic growth phase. For the Noc2-TAP P_{GAL1}-Rlp7 strain, a preparatory culture of 500 mL YPGal was grown to a late logarithmic phase. The two main cultures (YPD and YPGal) were then inoculated with an appropriate volume of the preparatory culture to allow logarithmic growth for 16 h before harvesting (Sahasranaman et al. 2011). Additionally, some cells were treated with 0.2 M lithium chloride (sterile filtered) for 3 h before cell harvesting (Dichtl et al. 1997). Cells were harvested by centrifugation at 6000*g* for 3 min at 4°C with the JLA 81000 rotor in a Beckmann centrifuge. Cells were washed with 20 mL ice-cold water and centrifuged at 1250*g* for 10 min at 4°C.

Purification

For particle isolation, cell pellets were resuspended in one volume of lysis buffer with protease inhibitors (20 mM HEPES, 10 mM KCl, 2.5 mM $MgCl_2$, and 1 mM EGTA pH 7.5 with 1 mM DTT, 0.5 mM PMSF, and 1 × FY-protease inhibitor [Serva]), followed by breaking the cells in the presence of 1.5 volumes of 0.6-mm glass beads (Sartorius AG) for 4 min in a bead mill (Merkenschlager). To remove dissoluble debris, centrifugation for 30 min at 4°C with 41,000*g* was performed. Before incubation of the resulting crude extract with self-coupled magnetic IgG beads for 90 min, 20 µL aliquots for protein and RNA analysis were taken (Oeffinger et al. 2007; Ohmayer et al. 2013; Zisser et al. 2018). After five washing steps using lysis buffer with 1 mM DTT, one-fifth of the bead volume was removed and stored for RNA analysis (= pull-down). Pre-ribosomal particles were eluted from the beads with purified TEV protease in lysis buffer with 100 mM NaCl and 1 mM DTT. The resulting TEV eluates were analyzed by SDS-PAGE and western blot.

SDS-PAGE and western blot

Proteins were separated in 4%–12% SDS-PAGE gels (NuPAGE Bis-Tris, Invitrogen) and visualized using the Colloidal Blue Staining Kit (Invitrogen).

When used for western blots, proteins were transferred from the gel on a polyvinylidene fluoride membrane (Carl Roth GmbH) in CAPS transfer buffer (10 mM CAPS, 10% methanol, pH 11). All antibodies were diluted as indicated in Supplemental Table S4 in 1× TST buffer (50 mM Tris, 0.1% Tween20, 0.15% NaCl, pH 7.4) with 1% milk powder. Detection of the chemiluminescence signal was performed with the Western blot Detection Reagent (Clarity Bio-Rad) on a ChemiDoc Touch Imaging System (Bio-Rad).

Proteolysis and LC–MS/MS measurement

Proteins were digested with LysC and trypsin with a filter-aided sample preparation (FASP) protocol as described (Wiśniewski et al. 2009; Grosche et al. 2016). Eluted peptides were acidified with TFA before LC–MS/MS measurement on a QExactive HF-X mass spectrometer (Thermo Fisher Scientific) coupled online to a Ultimate 3000 RSLC nano-HPLC (Dionex). Peptides were loaded onto the C18 trap column, eluted, and separated on the C18 reversed-phase analytical column (nanoEase MZ HSS T3, 100 Å, 1.8 µm, 75 µm × 250 mm; Waters) in a 95-min nonlinear acetonitrile gradient from 5% to 40% at a flow rate of 250 nL/min. MS spectra were recorded at a resolution of 60,000 with an automatic gain control (AGC) target of 3×10^6 and a maximum injection time of 30 msec from 300 to 1500 *m/z*. From the MS scan, the 15 most abundant peptide ions were selected for fragmentation via HCD with a normalized collision energy of 28, an isolation window of 1.6 *m/z*, and a dynamic exclusion of 30 sec. MS/MS spectra were recorded at a resolution of 15,000 with an AGC target of 1×10^5 and a maximum injection time of 50 msec. Unassigned charges and charges of +1 and >+8 were excluded from the precursor selection. The mass spectrometry proteomics data have been deposited to the ProteomeXchange Consortium via the PRIDE (Perez-Riverol et al. 2022) partner repository with the data set identifier PXD047506.

Protein identification and label-free quantification of proteomic data

Acquired raw files were analyzed in the Proteome Discoverer software (version 2.5, Thermo Fisher Scientific) for peptide and protein identification and quantification. A database search was performed using the Sequest HT search engine against the UniProt Yeast database (6637 sequences, 3,025,003 residues), considering full tryptic specificity, allowing for up to one missed cleavage, a precursor mass tolerance of 10 ppm, and a fragment mass tolerance of 0.02 Da. Carbamidomethylation of cysteine was set as a static modification and deamidation of asparagine and glutamine, oxidation of methionine, and a combination of methionine loss with acetylation on protein N terminus were allowed as dynamic modifications. The Percolator algorithm (Käll et al. 2007) was used for validating peptide spectrum matches and peptides. Quantification of proteins was based on summed peptide abundances for the TOP3 unique peptides per protein with an XCorr score > 1 and a peptide FDR < 1%. Peptide abundance values

were normalized on the total peptide amount per sample. Match-between runs for label-free quantification was limited to a retention time window of 1 min and a mass shift of 0.5 ppm. Resulting protein abundances were filtered for a protein FDR of 1% and by unambiguous identification and quantification during prior steps. For TOP3 stoichiometry calculations, proteins matching the criteria of three found peptides per protein were included (Supplemental Excel Sheet S1; Silva et al. 2006; Fabre et al. 2014). The abundance of each of those proteins was related to the abundance of the Noc2 bait protein. The mean and standard deviation (SD) of the relative abundance to the bait was calculated for two biological replicates. After filtering for a SD of <10%, we included 46 proteins with an abundance of at least 20% (0.2) relative to the bait to be the most likely candidates of Noc2 copurifying proteins.

RNA isolation

Total RNA was extracted from cells grown in 1 mL medium to late exponential growth phase. Cells were resuspended in 500 µL RNA lysis buffer (10 mM Tris, 10 mM EDTA, 0.5% SDS, pH 7.5) and lysed in the presence of 200 µL 0.6-mm glass beads (Sartorius AG) by shaking for 4 min in the Mini-Beadbeater-96 (Biospec Products). The RNA of the resulting cell extract (= total RNA), from crude extract or washed magnetic IgG beads from TAP purifications (= pull-down, see above) was isolated by phenol, chloroform, and isoamylalcohol extraction (P:C:I, 25:24:1). As an aqueous phase, RNA lysis buffer was used, and RNA was precipitated with absolute ethanol and sodium acetate. Subsequently, the RNA pellet was dissolved in nuclease-free water (Fresenius). RNA concentration and quality were determined using OD_{260} and OD_{280} measurements. If the RNA sample was used for northern blotting, it was prepared with 5× RNA loading dye (0.16% bromophenol blue, 4 mM EDTA, 0.98% formaldehyde, 17.4% glycerol, 30.38% formamide, 40% 10× MOPS [see northern blot]) to 1× concentration. For Riboprobing, RNA samples were stored in nuclease-free water at −80°C.

Northern blot

RNA prepared as described above was denatured for 10 min at 65°C and separated at 60 V for 7–8 h on a 1.5% agarose gel (containing 0.01% ethidium bromide, 0.75% formaldehyde and 1× MOPS [20 mM 3-(N-morpholino) propanesulfonic acid, 5 mM sodium acetate, 1 mM EDTA pH 7.0]). The separated RNA was transferred overnight onto Hybond-N+ nylon membranes (GE Healthcare) by capillary transfer in 20× SSC (3 M NaCl, 0.3 M Na_3 citrate). Hybridization with ^{32}P 5′-radiolabeled oligonucleotides (see Supplemental Table S3) was performed overnight at 42°C (37°C for EC_2) in hybridization buffer (0.5 M Na_2HPO_4, 7% SDS, 1 mM EDTA, pH 7.2). After three subsequent washing steps with washing buffer (40 mM Na_2HPO_4, 1% SDS, pH 7.2), signals were detected by exposing X-ray films. Membranes were recovered before the next hybridization using 1% SDS solution.

Riboprobing

"Riboprobing" describes the here presented combination of RNA ligation and cDNA synthesis with subsequent amplification using rRNA-specific primers. All detailed reaction conditions are provided in Supplemental Table S5.

RNA ligase reaction

RNA ligation linkers were specifically designed for either 3′ or 5′ end RNA ligation (see Supplemental Table S3) using the T4 RNA Ligase (NEB) in the presence of RiboLock RNAse inhibitor (Thermo Fischer). The resulting linker-RNA products were purified with the RNeasy Clean-up Kit (QIAGEN).

cDNA synthesis

The purified linker-RNA product served as template for a reverse transcription reaction with SuperScript III (Thermo Fischer) in the presence of RNaseOUT Recombinant RNase Inhibitor (Thermo Fischer). Primers are listed in Supplemental Table S3.

PCR

Initially, different amounts (1/50 to 1/3) of the obtained cDNA were tested as template for PCR amplification. We found that 1/13 of the generated cDNA gave the highest PCR yield using different primer pairs listed in the Supplemental Table S3.

Analysis

PCR products were separated in 1.5% agarose gels (containing 40 mM Tris-acetate and 1 mM EDTA pH 8). DNA fragments were visualized with ethidium bromide staining and UV light irradiation using a ChemiDoc XRS + device (Bio-Rad Laboratories) and the Image Lab 6.0.1 software (Bio-Rad Laboratories). DNA bands were cut out of the agarose gel and the DNA was extracted with the Monarch Gel Extraction Kit (NEB) or GeneJET Gel Extraction Kit (Thermo Fisher).

Purified DNA was sent for Sanger sequencing to Eurofins Genomics or Microsynth with one of the amplification primers. Sequences were analyzed with Serial Cloner and SnapGeneViewer (Dotmatics; available at snapgene.com). The full sequence of the 35S pre-rRNA of *S. cerevisiae* was downloaded from RNAcentral (ID: URS00004BEF81_559292).

Quantification of Riboprobing and northern blot signals

Signals of the exposed X-ray films (northern blot) or 1.5% agarose gel images (Riboprobing) were quantified with the Image Lab 6.0.1 software (Bio-Rad Laboratories). For both experimental approaches, two independent replicates were quantified.

To quantify the Riboprobing experiment, the bands arising from the three 27S pre-rRNA species were summed up to obtain the $27S_{total}$ pre-rRNA signal. To compare the different investigated samples, we calculated the ratio of the individual 27S pre-rRNA species (each single signal) in each sample to the $27S_{total}$ pre-rRNA signal (summed-up signal) in the untreated wild-type condition sample. To calculate the proportion of $27SA_2$ pre-rRNA, the signal for $27SA_2$ pre-rRNA was related to the $27S_{total}$ pre-rRNA signal (summed up signal) within each sample.

For northern blots, the signals for $27S_{total}$ pre-rRNA (EC_2 probe) were related to the signals for the $27SA_2$ pre-rRNA (A_2A_3 probe)

after relating the signals to the 35S pre-rRNA signals of both probes. The normalized values of the two different probes were then used to compare the different samples as described for Riboprobing: Each signal was related to the $27S_{total}$ pre-rRNA signal of the untreated wild-type condition, as well as the proportion of $27SA_2$ pre-rRNA to $27S_{total}$ pre-rRNA.

DATA DEPOSITION

The data of this article will be shared by the corresponding author upon request. The mass spectrometry proteomics data have been deposited to the ProteomeXchange Consortium via the PRIDE (Perez-Riverol et al. 2022) partner repository with the data set identifier PXD047506.

SUPPLEMENTAL MATERIAL

Supplemental material is available for this article.

ACKNOWLEDGMENTS

We thank Michael Prattes and Kai-Uwe Fröhlich for carefully reading and commenting on the manuscript. We thank Brigitte Pertschy, John L. Woolford, Jr., Michael A. McAlear, Micheline Fromont-Racin, Philipp Milkereit, Arlen W. Johnson, David Tollervey, Melanie Oaks, Sabine Rospert, Matthias Seedorf, Ed Hurt, and Jesus de la Cruz for sharing strains or providing antibodies. We thank the members of the Bergler laboratory and the Pertschy laboratory for helpful discussions. The work was supported by the Austrian Science Foundation (FWF) grants 29451, 32536, and 32977 (to H.B.).

Author contributions: H.B., L.K., and M.G. designed the study. H.B. and M.G. planned the experiments. M.G. and G.Z. generated strains. M.G. purified pre-ribosomal particles. M.G. did the RNA isolation, the Riboprobing experiments, and the northern blots. J.M.-P. and S.M.H. performed the qMS analysis. M.G. generated the figures. M.G. and H.B. wrote the manuscript. All authors read and approved the final version of the manuscript.

Received December 5, 2023; accepted March 16, 2024.

REFERENCES

Allmang C, Mitchell P, Petfalski E, Tollervey D. 2000. Degradation of ribosomal RNA precursors by the exosome. *Nucleic Acids Res* **28:** 1684–1691. doi:10.1093/nar/28.8.1684

Awad D, Prattes M, Kofler L, Rössler I, Loibl M, Pertl M, Zisser G, Wolinski H, Pertschy B, Bergler H. 2019. Inhibiting eukaryotic ribosome biogenesis. *BMC Biol* **17:** 46. doi:10.1186/s12915-019-0664-2

Baßler J, Hurt E. 2019. Eukaryotic ribosome assembly. *Annu Rev Biochem* **88:** 281–306. doi:10.1146/annurev-biochem-013118-110817

Bernstein KA, Gallagher JEG, Mitchell BM, Granneman S, Baserga SJ. 2004. The small-subunit processome is a ribosome assembly intermediate. *Eukaryot Cell* **3:** 1619–1626. doi:10.1128/EC.3.6.1619-1626.2004

Bleichert F, Granneman S, Osheim YN, Beyer AL, Baserga SJ. 2006. The PINc domain protein Utp24, a putative nuclease, is required for the early cleavage steps in 18S rRNA maturation. *Proc Natl Acad Sci* **103:** 9464–9469. doi:10.1073/pnas.0603673103

Boissier F, Schmidt CM, Linnemann J, Fribourg S, Perez-Fernandez J. 2017. Pwp2 mediates UTP-B assembly via two structurally independent domains. *Sci Rep* **7:** 3169. doi:10.1038/s41598-017-03034-y

Briggs MW, Burkard KT, Butler JS. 1998. Rrp6p, the yeast homologue of the human PM-Scl 100-kDa autoantigen, is essential for efficient 5.8 S rRNA 3′ end formation. *J Biol Chem* **273:** 13255–13263. doi:10.1074/jbc.273.21.13255

Carey MF, Peterson CL, Smale ST. 2013. The primer extension assay. *Cold Spring Harb Protoc* **2013:** pdb.prot071902. doi:10.1101/pdb.prot071902

Castle CD, Sardana R, Dandekar V, Borgianini V, Johnson AW, Denicourt C. 2013. Las1 interacts with Grc3 polynucleotide kinase and is required for ribosome synthesis in *Saccharomyces cerevisiae*. *Nucleic Acids Res* **41:** 1135–1150. doi:10.1093/nar/gks1086

Catez F, Dalla Venezia N, Marcel V, Zorbas C, Lafontaine DLJ, Diaz J-J. 2019. Ribosome biogenesis: an emerging druggable pathway for cancer therapeutics. *Biochem Pharmacol* **159:** 74–81. doi:10.1016/j.bcp.2018.11.014

Cheng J, Lau B, La Venuta G, Ameismeier M, Berninghausen O, Hurt E, Beckmann R. 2020. 90S pre-ribosome transformation into the primordial 40S subunit. *Science* **369:** 1470–1476. doi:10.1126/science.abb4119

Delprato A, Al Kadri Y, Pérébaskine N, Monfoulet C, Henry Y, Henras AK, Fribourg S. 2014. Crucial role of the Rcl1p-Bms1p interaction for yeast pre-ribosomal RNA processing. *Nucleic Acids Res* **42:** 10161–10172. doi:10.1093/nar/gku682

Dichtl B, Stevens A, Tollervey D. 1997. Lithium toxicity in yeast is due to the inhibition of RNA processing enzymes. *EMBO J* **16:** 7184–7195. doi:10.1093/emboj/16.23.7184

Dielforder T, Braun CM, Hölzgen F, Li S, Thiele M, Huber M, Ohmayer U, Perez-Fernandez J. 2022. Structural probing with MNase tethered to ribosome assembly factors resolves flexible RNA regions within the nascent pre-ribosomal RNA. *Noncoding RNA* **8:** 1. doi:10.3390/ncrna8010001

Dörner K, Ruggeri C, Zemp I, Kutay U. 2023. Ribosome biogenesis factors—from names to functions. *EMBO J* **42:** e112699. doi:10.15252/embj.2022112699

Dragon F, Gallagher JEG, Compagnone-Post PA, Mitchell BM, Porwancher KA, Wehner KA, Wormsley S, Settlage RE, Shabanowitz J, Osheim Y, et al. 2002. A large nucleolar U3 ribonucleoprotein required for 18S ribosomal RNA biogenesis. *Nature* **417:** 967–970. doi:10.1038/nature00769

Dunbar DA, Dragon F, Lee SJ, Baserga SJ. 2000. A nucleolar protein related to ribosomal protein L7 is required for an early step in large ribosomal subunit biogenesis. *Proc Natl Acad Sci* **97:** 13027–13032. doi:10.1073/pnas.97.24.13027

Durand S, Bruelle M, Bourdelais F, Bennychen B, Blin-Gonthier J, Isaac C, Huyghe A, Martel S, Seyve A, Vanbelle C, et al. 2023. RSL24D1 sustains steady-state ribosome biogenesis and pluripotency translational programs in embryonic stem cells. *Nat Commun* **14:** 356. doi:10.1038/s41467-023-36037-7

Dziembowski A, Lorentzen E, Conti E, Séraphin B. 2007. A single subunit, Dis3, is essentially responsible for yeast exosome core activity. *Nat Struct Mol Biol* **14:** 15–22. doi:10.1038/nsmb1184

Esakova O, Perederina A, Berezin I, Krasilnikov AS. 2013. Conserved regions of ribonucleoprotein ribonuclease MRP are involved in interactions with its substrate. *Nucleic Acids Res* **41:** 7084–7091. doi:10.1093/nar/gkt432

Faber AW, Vos HR, Vos JC, Raué HA. 2006. 5′-end formation of yeast 5.8SL rRNA is an endonucleolytic event. *Biochem Biophys Res Commun* **345:** 796–802. doi:10.1016/j.bbrc.2006.04.166

Fabre B, Lambour T, Bouyssié D, Menneteau T, Monsarrat B, Burlet-Schiltz O, Bousquet-Dubouch M-P. 2014. Comparison of label-

free quantification methods for the determination of protein complexes subunits stoichiometry. *EuPA Open Proteom* **4:** 82–86. doi:10.1016/j.euprot.2014.06.001

Fatica A, Oeffinger M, Dlakić M, Tollervey D. 2003. Nob1p is required for cleavage of the 3′ end of 18S rRNA. *Mol Cell Biol* **23:** 1798–1807. doi:10.1128/MCB.23.5.1798-1807.2003

Fatica A, Tollervey D, Dlakić M. 2004. PIN domain of Nob1p is required for D-site cleavage in 20S pre-rRNA. *RNA* **10:** 1698–1701. doi:10.1261/rna.7123504

Frohman MA, Dush MK, Martin GR. 1988. Rapid production of full-length cDNAs from rare transcripts: amplification using a single gene-specific oligonucleotide primer. *Proc Natl Acad Sci* **85:** 8998–9002. doi:10.1073/pnas.85.23.8998

Fromm L, Falk S, Flemming D, Schuller JM, Thoms M, Conti E, Hurt E. 2017. Reconstitution of the complete pathway of ITS2 processing at the pre-ribosome. *Nat Commun* **8:** 1787. doi:10.1038/s41467-017-01786-9

Fuchs RT, Sun Z, Zhuang F, Robb GB. 2015. Bias in ligation-based small RNA sequencing library construction is determined by adaptor and RNA structure. *PLoS ONE* **10:** e0126049. doi:10.1371/journal.pone.0126049

Gasse L, Flemming D, Hurt E. 2015. Coordinated ribosomal ITS2 RNA processing by the Las1 complex integrating endonuclease, polynucleotide kinase, and exonuclease activities. *Mol Cell* **60:** 808–815. doi:10.1016/j.molcel.2015.10.021

Geerlings TH, Vos JC, Raué HA. 2000. The final step in the formation of 25S rRNA in *Saccharomyces cerevisiae* is performed by 5′→3′ exonucleases. *RNA* **6:** 1698–1703. doi:10.1017/S1355838200001540

Granneman S, Petfalski E, Tollervey D. 2011. A cluster of ribosome synthesis factors regulate pre-rRNA folding and 5.8S rRNA maturation by the Rat1 exonuclease. *EMBO J* **30:** 4006–4019. doi:10.1038/emboj.2011.256

Grosche A, Hauser A, Lepper MF, Mayo R, von Toerne C, Merl-Pham J, Hauck SM. 2016. The proteome of native adult Müller glial cells from murine retina. *Mol Cell Proteomics* **15:** 462–480. doi:10.1074/mcp.M115.052183

Henry Y, Wood H, Morrissey JP, Petfalski E, Kearsey S, Tollervey D. 1994. The 5′ end of yeast 5.8S rRNA is generated by exonucleases from an upstream cleavage site. *EMBO J* **13:** 2452–2463. doi:10.1002/j.1460-2075.1994.tb06530.x

Heuer A, Thomson E, Schmidt C, Berninghausen O, Becker T, Hurt E, Beckmann R. 2017. Cryo-EM structure of a late pre-40S ribosomal subunit from *Saccharomyces cerevisiae*. *eLife* **6:** e30189. doi:10.7554/eLife.30189

Hierlmeier T, Merl J, Sauert M, Perez-Fernandez J, Schultz P, Bruckmann A, Hamperl S, Ohmayer U, Rachel R, Jacob A, et al. 2013. Rrp5p, Noc1p and Noc2p form a protein module which is part of early large ribosomal subunit precursors in *S. cerevisiae*. *Nucleic Acids Res* **41:** 1191–1210. doi:10.1093/nar/gks1056

Horn DM, Mason SL, Karbstein K. 2011. Rcl1 protein, a novel nuclease for 18 S ribosomal RNA production. *J Biol Chem* **286:** 34082–34087. doi:10.1074/jbc.M111.268649

Hunziker M, Barandun J, Buzovetsky O, Steckler C, Molina H, Klinge S. 2019. Conformational switches control early maturation of the eukaryotic small ribosomal subunit. *eLife* **8:** e45185. doi:10.7554/eLife.45185

Janke C, Magiera MM, Rathfelder N, Taxis C, Reber S, Maekawa H, Moreno-Borchart A, Doenges G, Schwob E, Schiebel E, et al. 2004. A versatile toolbox for PCR-based tagging of yeast genes: new fluorescent proteins, more markers and promoter substitution cassettes. *Yeast* **21:** 947–962. doi:10.1002/yea.1142

Käll L, Canterbury JD, Weston J, Noble WS, MacCoss MJ. 2007. Semi-supervised learning for peptide identification from shotgun proteomics datasets. *Nat Methods* **4:** 923–925. doi:10.1038/nmeth1113

Kevil CG, Wlash L, Laroux FS, Kalogeris T, Grisham MB, Alexander JS. 1997. An improved, rapid northern protocol. *Biochem Biophys Res Commun* **238:** 277–279. doi:10.1006/bbrc.1997.7284

Khoshnevis S, Liu X, Dattolo MD, Karbstein K. 2019. Rrp5 establishes a checkpoint for 60S assembly during 40S maturation. *RNA* **25:** 1164–1176. doi:10.1261/rna.071225.119

Klinge S, Woolford JL. 2019. Ribosome assembly coming into focus. *Nat Rev Mol Cell Biol* **20:** 116–131. doi:10.1038/s41580-018-0078-y

Koš M, Tollervey D. 2010. Yeast pre-rRNA processing and modification occur cotranscriptionally. *Mol Cell* **37:** 809–820. doi:10.1016/j.molcel.2010.02.024

Li X, Zengel JM, Lindahl L. 2021. A novel model for the RNase MRP-induced switch between the formation of different forms of 5.8S rRNA. *Int J Mol Sci* **22:** 6690. doi:10.3390/ijms22136690

Lindahl L, Bommankanti A, Li X, Hayden L, Jones A, Khan M, Oni T, Zengel JM. 2009. RNase MRP is required for entry of 35S precursor rRNA into the canonical processing pathway. *RNA* **15:** 1407–1416. doi:10.1261/rna.1302909

Longtine MS, Mckenzie A III, Demarini DJ, Shah NG, Wach A, Brachat A, Philippsen P, Pringle JR. 1998. Additional modules for versatile and economical PCR-based gene deletion and modification in *Saccharomyces cerevisiae*. *Yeast* **14:** 953–961. doi:10.1002/(SICI)1097-0061(199807)14:10<953::AID-YEA293>3.0.CO;2-U

Lygerou Z, Allmang C, Tollervey D, Séraphin B. 1996. Accurate processing of a eukaryotic precursor ribosomal RNA by ribonuclease MRP in vitro. *Science* **272:** 268–270. doi:10.1126/science.272.5259.268

Milkereit P, Gadal O, Podtelejnikov A, Trumtel S, Gas N, Petfalski E, Tollervey D, Mann M, Hurt E, Tschochner H. 2001. Maturation and intranuclear transport of pre-ribosomes requires Noc proteins. *Cell* **105:** 499–509. doi:10.1016/S0092-8674(01)00358-0

Mitchell P, Petfalski E, Shevchenko A, Mann M, Tollervey D. 1997. The exosome: a conserved eukaryotic RNA processing complex containing multiple 3′→5′ exoribonucleases. *Cell* **91:** 457–466. doi:10.1016/S0092-8674(00)80432-8

Mitterer V, Pertschy B. 2022. RNA folding and functions of RNA helicases in ribosome biogenesis. *RNA Biol* **19:** 781–810. doi:10.1080/15476286.2022.2079890

Mitterer V, Thoms M, Buschauer R, Berninghausen O, Hurt E, Beckmann R. 2023. Concurrent remodelling of nucleolar 60S subunit precursors by the Rea1 ATPase and Spb4 RNA helicase. *eLife* **12:** e84877. doi:10.7554/eLife.84877

Ni C, Schmitz DA, Lee J, Pawłowski K, Wu J, Buszczak M. 2022. Labeling of heterochronic ribosomes reveals C1ORF109 and SPATA5 control a late step in human ribosome assembly. *Cell Rep* **38:** 110597. doi:10.1016/j.celrep.2022.110597

Oeffinger M, Wei KE, Rogers R, DeGrasse JA, Chait BT, Aitchison JD, Rout MP. 2007. Comprehensive analysis of diverse ribonucleoprotein complexes. *Nat Methods* **4:** 951–956. doi:10.1038/nmeth1101

Oeffinger M, Zenklusen D, Ferguson A, Wei KE, El Hage A, Tollervey D, Chait BT., Singer RH, Rout MP. 2009. Rrp17p is a eukaryotic exonuclease required for 5′ end processing of Pre-60S ribosomal RNA. *Mol Cell* **36:** 768–781. doi:10.1016/j.molcel.2009.11.011

Ohmayer U, Gamalinda M, Sauert M, Ossowski J, Pöll G, Linnemann J, Hierlmeier T, Perez-Fernandez J, Kumcuoglu B, Leger-Silvestre I, et al. 2013. Studies on the assembly characteristics of large subunit ribosomal proteins in *S. cerevisiae*. *PLoS ONE* **8:** e68412. doi:10.1371/journal.pone.0068412

Osheim YN, French SL, Keck KM, Champion EA, Spasov K, Dragon F, Baserga SJ, Beyer AL. 2004. Pre-18S ribosomal RNA is structurally compacted into the SSU processome prior to being cleaved from nascent transcripts in *Saccharomyces cerevisiae*. *Mol Cell* **16:** 943–954. doi:10.1016/j.molcel.2004.11.031

Perez-Riverol Y, Bai J, Bandla C, García-Seisdedos D, Hewapathirana S, Kamatchinathan S, Kundu DJ, Prakash A, Frericks-Zipper A, Eisenacher M, et al. 2022. The PRIDE database resources in 2022: a hub for mass spectrometry-based proteomics evidences. *Nucleic Acids Res* **50:** D543–D552. doi:10.1093/nar/gkab1038

Pertschy B, Schneider C, Gnädig M, Schäfer T, Tollervey D, Hurt E. 2009. RNA helicase Prp43 and its co-factor Pfa1 promote 20 to 18 S rRNA processing catalyzed by the endonuclease Nob1. *J Biol Chem* **284:** 35079–35091. doi:10.1074/jbc.M109.040774

Pillon MC, Hsu AL, Krahn JM, Williams JG, Goslen KH, Sobhany M, Borgnia MJ, Stanley RE. 2019. Cryo-EM reveals active site coordination within a multienzyme pre-rRNA processing complex. *Nat Struct Mol Biol* **26:** 830–839. doi:10.1038/s41594-019-0289-8

Pillon MC, Goslen KH, Gordon J, Wells ML, Williams JG, Stanley RE. 2020. It takes two (Las1 HEPN endoribonuclease Domains) to cut RNA correctly. *J Biol Chem* **295:** 5857–5870. doi:10.1074/jbc.RA119.011193

Sahasranaman A, Dembowski J, Strahler J, Andrews P, Maddock J, Woolford JL. 2011. Assembly of *Saccharomyces cerevisiae* 60S ribosomal subunits: role of factors required for 27S pre-rRNA processing. *EMBO J* **30:** 4020–4032. doi:10.1038/emboj.2011.338

Sailer C, Jansen J, Sekulski K, Cruz VE, Erzberger JP, Stengel F. 2022. A comprehensive landscape of 60S ribosome biogenesis factors. *Cell Rep* **38:** 110353. doi:10.1016/j.celrep.2022.110353

Sanghai ZA, Piwowarczyk R, Broeck AV, Klinge S. 2023. A co-transcriptional ribosome assembly checkpoint controls nascent large ribosomal subunit maturation. *Nat Struct Mol Biol* **30:** 594–599. doi:10.1038/s41594-023-00947-3

Schneider C, Bohnsack KE. 2023. Caught in the act-visualizing ribonucleases during eukaryotic ribosome assembly. *Wiley Interdiscip Rev RNA* **14:** e1766. doi:10.1002/wrna.1766

Schuller JM, Falk S, Fromm L, Hurt E, Conti E. 2018. Structure of the nuclear exosome captured on a maturing preribosome. *Science* **360:** 219–222. doi:10.1126/science.aar5428

Silva JC, Gorenstein MV, Li G-Z, Vissers JPC, Geromanos SJ. 2006. Absolute quantification of proteins by LCMSE: a virtue of parallel MS acquisition. *Mol Cell Proteomics* **5:** 144–156. doi:10.1074/mcp.M500230-MCP200

Sloan KE, Warda AS, Sharma S, Entian K-D, Lafontaine DLJ, Bohnsack MT. 2017. Tuning the ribosome: the influence of rRNA modification on eukaryotic ribosome biogenesis and function. *RNA Biol* **14:** 1138–1152. doi:10.1080/15476286.2016.1259781

Streit S, Michalski CW, Erkan M, Kleeff J, Friess H. 2009. Northern blot analysis for detection and quantification of RNA in pancreatic cancer cells and tissues. *Nat Protoc* **4:** 37–43. doi:10.1038/nprot.2008.216

Thomson E, Tollervey D. 2010. The final step in 5.8S rRNA processing is cytoplasmic in *Saccharomyces cerevisiae*. *Mol Cell Biol* **30:** 976–984. doi:10.1128/MCB.01359-09

Tomecki R, Sikorski PJ, Zakrzewska-Placzek M. 2017. Comparison of preribosomal RNA processing pathways in yeast, plant and human cells - focus on coordinated action of endo- and exoribonucleases. *FEBS Lett* **591:** 1801–1850. doi:10.1002/1873-3468.12682

Vanden Broeck A, Klinge S. 2023. Principles of human pre-60S biogenesis. *Science* **381:** eadh3892. doi:10.1126/science.adh3892

van Hoof A, Lennertz P, Parker R. 2000. Three conserved members of the RNase D family have unique and overlapping functions in the processing of 5S, 5.8S, U4, U5, RNase MRP and RNase P RNAs in yeast. *EMBO J* **19:** 1357–1365. doi:10.1093/emboj/19.6.1357

Venema J, Planta RJ, Raué HA. 1998. In vivo mutational analysis of ribosomal RNA in *Saccharomyces cerevisiae*. *Methods Mol Biol* **77:** 257–270. doi:10.1385/0-89603-397-X:257

Wells GR, Weichmann F, Colvin D, Sloan KE, Kudla G, Tollervey D, Watkins NJ, Schneider C. 2016. The PIN domain endonuclease Utp24 cleaves pre-ribosomal RNA at two coupled sites in yeast and humans. *Nucleic Acids Res* **44:** 5399–5409. doi:10.1093/nar/gkw213

Wiśniewski JR, Zougman A, Nagaraj N, Mann M. 2009. Universal sample preparation method for proteome analysis. *Nat Methods* **6:** 359–362. doi:10.1038/nmeth.1322

Wu S, Tutuncuoglu B, Yan K, Brown H, Zhang Y, Tan D, Gamalinda M, Yuan Y, Li Z, Jakovljevic J, et al. 2016. Diverse roles of assembly factors revealed by structures of late nuclear pre-60S ribosomes. *Nature* **534:** 133–137. doi:10.1038/nature17942

Zhuang F, Fuchs RT, Sun Z, Zheng Y, Robb GB. 2012. Structural bias in T4 RNA ligase-mediated 3′-adapter ligation. *Nucleic Acids Res* **40:** e54. doi:10.1093/nar/gkr1263

Zisi A, Bartek J, Lindström MS. 2022. Targeting ribosome biogenesis in cancer: lessons learned and way forward. *Cancers* **14:** 2126. doi:10.3390/cancers14092126

Zisser G, Ohmayer U, Mauerhofer C, Mitterer V, Klein I, Rechberger GN, Wolinski H, Prattes M, Pertschy B, Milkereit P, et al. 2018. Viewing pre-60S maturation at a minute's timescale. *Nucleic Acids Res* **46:** 3140–3151. doi:10.1093/nar/gkx1293

MEET THE FIRST AUTHOR

Magdalena Gerhalter

***Meet the First Author(s)* is an editorial feature within *RNA*, in which the first author(s) of research-based papers in each issue have the opportunity to introduce themselves and their work to readers of *RNA* and the RNA research community. Magdalena Gerhalter is the first author of this paper, "The novel pre-rRNA detection workflow 'Riboprobing' allows simple identification of undescribed RNA species." Magdalena is a PhD student in the laboratory of Helmut Bergler at the University of Graz in the Institute of Molecular Biosciences. Her research focuses on ribosome biogenesis, mainly of the large subunit.**

Continued

What are the major results described in your paper and how do they impact this branch of the field?

We developed a method that allows easy and quick analysis of different pre-rRNA species. Until now, this had to be done by northern blot and primer extension, both of which are quite laborious and often require radioactivity. We hope that our method will help researchers in the field to rapidly screen mutants or inhibitors for defects in pre-rRNA processing.

What led you to study RNA or this aspect of RNA science?

During my bachelor's degree studies, my view of RNA fortunately changed from "DNA's single-stranded brother" to "an incredible molecule with an ancient evolutionary history that is involved in a wide variety of processes in the cell." Later, I focused on ribosome biogenesis, where I began to understand how pre-rRNA, snoRNPs, and hundreds of proteins work together to form a ribosome. During my PhD studies, I worked on projects that could not be analyzed sufficiently with northern blots, and I wondered if there was an easier way than a primer extension to solve this issue. We tried it, it worked, and we decided to share the workflow with the ribosome biogenesis community.

During the course of these experiments, were there any surprising results or particular difficulties that altered your thinking and subsequent focus?

We were most surprised by the drastic changes of pre-ribosomal particles that we observed after treatment with LiCl. We originally intended to use this compound as a proof of concept of our method, as the inhibitory effect of LiCl on RNase MRP was published by the Tollervey laboratory. We saw that treatment with LiCl resulted in an undescribed aberrant pre-rRNA that perfectly complements recent findings on RNase MRP.

If you were able to give one piece of advice to your younger self, what would that be?

At the beginning of your PhD, you think that three to four years is more than enough to work on all the exciting research questions of a project and to learn and master all the different methods that are useful for it. Take a deep breath and try to focus on a few points that you want to work on, because time flies.

What are your subsequent near- or long-term career plans?

I'm about to finish and defend my PhD and hope to continue working with RNA–protein complexes in my time as a postdoc, wherever that may be.

The novel pre-rRNA detection workflow "Riboprobing" allows simple identification of undescribed RNA species

Magdalena Gerhalter, Lisa Kofler, Gertrude Zisser, et al.

RNA 2024 30: 807-823 originally published online April 5, 2024
Access the most recent version at doi:10.1261/rna.079912.123